FULL PAPER

# Synthesis of Interfacially Active and Magnetically Responsive Nanoparticles for Multiphase Separation Applications

*Junxia Peng, Qingxia Liu, Zhenghe Xu,* and Jacob Masliyah*

**A novel interfacially active and magnetically responsive nanoparticle is designed and prepared by direct grafting of bromoesterified ethyl cellulose (EC-Br) onto the surface of amino-functionalized magnetite ($Fe_3O_4$) nanoparticles. Due to its strong interfacial activity, ethyl cellulose (EC) on the magnetic nanoparticles enables the EC-grafted $Fe_3O_4$ (M-EC) nanoparticles to be interfacially active. The grafting of interfacially active polymer EC on magnetic nanoparticles is confirmed by zeta-potential measurements, diffuse reflectance infrared Fourier-transform spectroscopic (DRIFTS) characterization, and thermogravimetric analysis (TGA). Scanning electron microscopy (SEM) images show a negligible increase in particle size, confirming the thin silica coating and grafted EC layer. The magnetization measurements show a marginal reduction in saturation magnetization by silica coating and EC grafting of original magnetic nanoparticles, confirming the presence of coatings. The M-EC nanoparticles prepared in this study show excellent interfacial activity and highly ordered features at the oil/water interface, as confirmed using the Langmuir–Blodgett technique and atomic force microscopy (AFM). The magnetic properties of M-EC nanoparticles at the oil/water interface make the interfacial properties tunable by or responsive to an external magnetic field. The occupancy of M-EC at the oil/water interface allows rapid separation of the water droplets from emulsions by an external magnetic field, demonstrating enhanced coalescence of magnetically tagged stable water droplets and a reduced overall volume fraction of the sludge.**

## 1. Introduction

Magnetic nanoparticles (MNPs), which are powerful markers and carriers for diverse research and industrial applications, have attracted a wide range of interest during the past two decades. Due to their magnetic responses to external magnetic field and convenient separation from a complex multiphase system by an external magnetic field,[1] MNPs with tailored surface functionalities have been widely used in life sciences, including biolabeling,[2] drug delivery,[3] biological cell and DNA separation,[4] contrast enhancement of magnetic resonance imaging,[5] protein purification,[6] and pathogen detection.[7] Industrial applications of functional MNPs include engineering of novel optical and electronic materials,[8] specialty catalysts,[9] and the removal of organic pollutant,[10] heavy metals from municipal water and industrial effluents and toxic trace elements from flue gases.[11] In addition, the magnetic nanofluids have been applied to the smart cooling devices in electronic apparatus and engines and the optical technique for the detection of surface defects in steel products.[12] The application of MNPs to separation and purification sciences is mainly dependent on the ability to modify their surfaces for desired functions. The most commonly used approaches are physical/chemical adsorption, self-assembly, and surface coating of desired materials.[13–17]

Most recently, research focus has been shifted to the synthesis of interfacially active MNPs. The interfacial activity of magnetic nanocomposite particles allows them to assemble at the liquid/liquid or air/water interface into 2D or 3D nanostructures,[18] which have wide applications in optical and electronic nanodevices. The liquid/liquid or air/water interface serves as a flexible soft substrate for the rapid and spontaneous self-assembly of interfacially active MNPs. Magnetic nanocomposite particles with biwettable characteristics are able to transfer from the bulk phase to immiscible liquid/liquid interfaces.[19] It is of paramount importance for these particles to be readily dispersed in the continuous phase for delivery and to have the ability to target specific species (dispersed phases) to be removed or recovered from the rest of the system. Great efforts have been made to render the MNPs transferrable from the organic phase to the aqueous phase by self-assembly of hydrophilic ligands on hydrophobic MNPs or by encapsulation of hydrophobic iron oxide nanoparticles by amphiphilic block copolymers.[20] Another important area of interest is the synthesis of magnetic nanocomposites with stimuli-responsive property to stabilize emulsions by the external stimulus.[21] There has been recently increasing interest in the use of magnetic particles to stabilize emulsions by so-called

J. Peng, Prof. Q. Liu, Prof. Z. Xu, Prof. J. Masliyah
Department of Chemical and Materials Engineering
University of Alberta
Edmonton, Alberta T6G 2V4, Canada
E-mail: zhenghe.xu@ualberta.ca

DOI: 10.1002/adfm.201102156

Pickering emulsion stabilization.[22] In many industrial applications, it is highly desirable to destabilize and/or separate stable multiphase emulsions. Richtering et al. proposed a magnetic microgel for the remote control of stability and the separation of oil in water emulsions.[21a] In this study, we report a novel, interfacially active MNP that is highly stable in the organic phase and able to attach to stable water droplets in an emulsion. The tagging of stable water droplets by the interfacially active MNPs allows magnetic responses of the tagged water droplets to an external magnetic field for the controlled movement and enhanced coalescence of stable water droplets, aiming at a rapid and effective phase separation by applying an external magnetic field.

To synthesize interfacially active MNPs, it is extremely important to choose desired grafting chemicals that allow the synthesized particles to be interfacially active for effective tagging of the dispersed droplets that are stabilized by protecting interfacial films.[23] This requires the grafting chemicals to be extremely interfacial active and able to break and penetrate the protecting interfacial films. Ethyl cellulose (EC) is a derivative of natural cellulose that has fascinating properties such as good solubility in organic solvents, good thermal and mechanical stability, good biocompatibility, natural degradation to nontoxic and readily excreted products, and low cost.[24] Recently, we reported an extremely high interfacial activity of EC that can adsorb at extremely stable toluene-diluted bitumen/water interfaces, leading to effective demulsification of water-in-diluted-bitumen emulsions by a displacement of the original interfacial materials.[25,26] With these proven attractive attributes, EC would be a good candidate for engineering interfacially active MNPs. The major challenge is how one could graft EC onto MNPs without altering the interfacial activity of EC. Here, we report the synthesis of EC-grafted $Fe_3O_4$ nanoparticles (M-EC) as an interfacially active and magnetically responsive nanoparticle. The key to successful synthesis of the desired M-EC is the preparation of MNP surface to be reactive with EC.

The concept of synthesizing M-EC nanoparticles is illustrated in **Figure 1**. In our approach, the $Fe_3O_4$ nanoparticles were first coated with a thin layer of silica using a dense liquid silica coating (DLSC) method[15] to protect MNPs and to make the surface amenable for further functionalization. The silica-coated MNPs are then modified by the silane coupling agent, 3-aminopropyltriethoxysilane (3-APTES),[27] to render the surface of amine functionality. It is necessary to modify EC in order to make EC reactive with amine groups on the surface. In this study, we take the advantage of esterification reaction between acryl halide (COBr) with hydroxyl (–OH) and replace some of hydroxyl groups of EC with 2-bromoisobutyryl bromide by a previously reported method to obtain bromoesterified EC (EC-Br).[28] The EC-Br is then chemically anchored on the amine-functionalized $Fe_3O_4$ nanoparticle ($Fe_3O_4$-$SiO_2$-$NH_2$) surface to form a polymer EC layer through chemical reaction between $–NH_2$ groups on the $Fe_3O_4$-$SiO_2$-$NH_2$ surface and bromine on the EC-Br, leading to formation of M-EC.

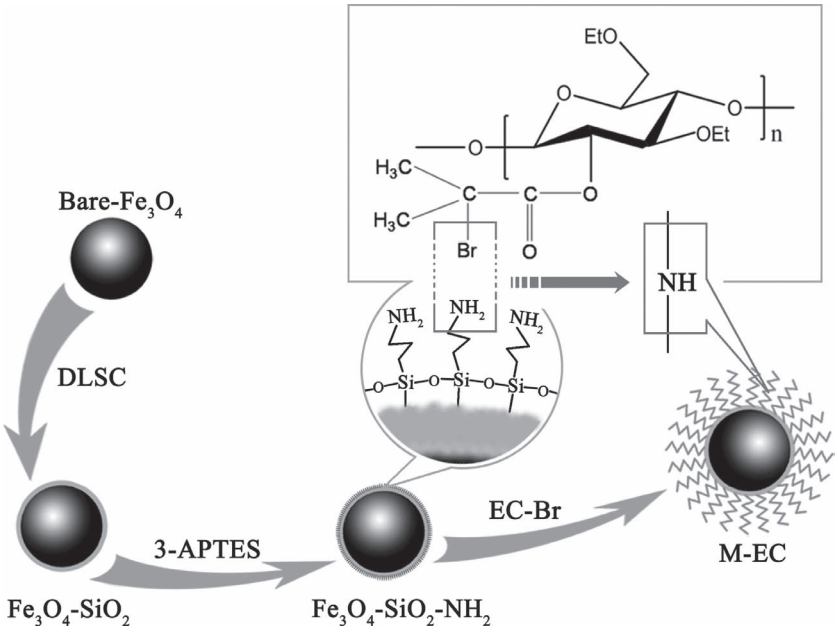


**Figure 1.** Schematic illustration of the synthesis procedures for M-EC nanoparticles.

As-prepared M-EC nanoparticles possess a strong magnetic core with an interfacially active organic EC layer on the surface. The interfacial activity of EC molecule brings M-EC dispersed in organic phase to the oil/water interface to tag the water droplets in emulsions, which allows them to be separated effectively by a magnetic separator. In M-EC, the $Fe_3O_4$ nanoparticles were protected from oxidation and acid leaching in real industrial applications by a thin layer of silica coating. The stability of M-EC provided with this protecting layer is one of the key features of M-EC for its recycle and regeneration in real applications. The advantage of this new approach is a shorter phase separation time and more effective separation with reduced oil loss and a small volume of waste sludge. The M-EC, as a magnetic demulsifier, can be recovered and reused. This is the first report of the synthesis of MNPs with an interfacially active EC layer to destabilize the water-in-oil (w/o) emulsions.

## 2. Results and Discussion

### 2.1. Characterization of M-EC Nanoparticles

#### *2.1.1. Scanning Electron Microscopy (SEM) Imaging*

**Figure 2** shows typical scanning electron microscopy (SEM) images of bare-$Fe_3O_4$ (Figure 2a) and M-EC (Figure 2b). Compared to bare-$Fe_3O_4$ nanoparticles, M-EC nanoparticles are much less aggregated as a result of surface modification by silica and polymer coatings. The distinct difference in particle aggregation with and without surface coating indicates that the grafting of naphtha-soluble EC on MNPs provides a steric

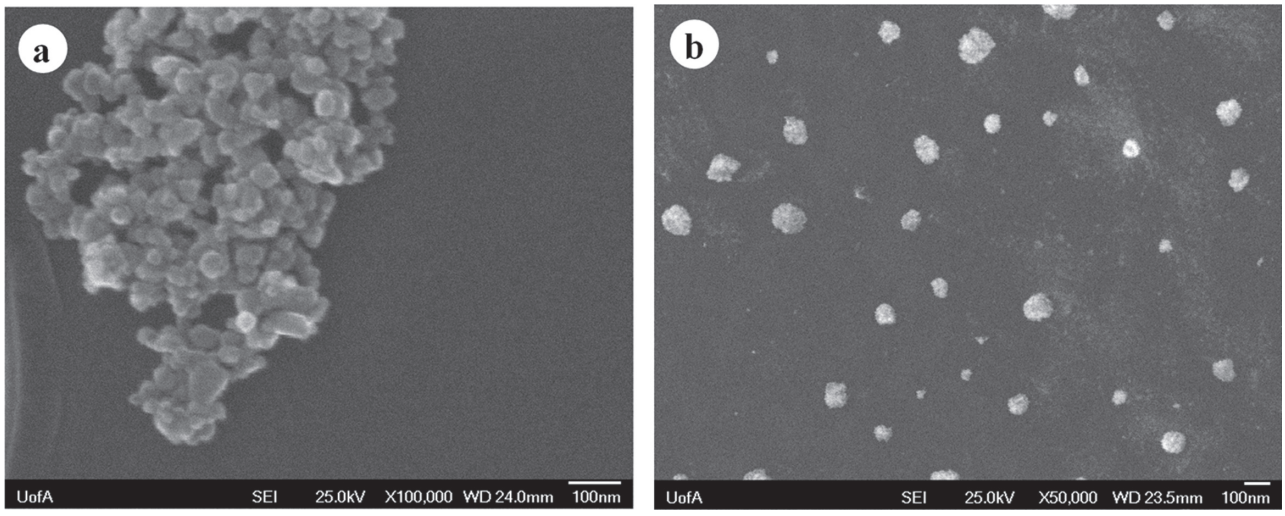


**Figure 2.** Field-emission SEM (FE-SEM) images of a) bare-$Fe_3O_4$ particles and b) silica-coated and EC-grafted $Fe_3O_4$ (M-EC) particles, showing minimized agglomeration of M-EC in comparison to the original MNPs.

repulsion to minimize the otherwise encountered aggregation of MNPs in organic solvent.

### 2.1.2. Zeta-Potential Measurements

The zeta potential of MNPs collected during the various stage of synthesis was determined in the same 1 mM KCl aqueous solution with a pH of 5.3 to provide a direct evidence of silica coating and EC grafting on the surface of the nanosized magnetite particles. The results in **Figure 3** show that in 1 mM KCl aqueous solutions with a pH of 5.3, the bare $Fe_3O_4$ nanoparticles are slightly positively charged with a mean zeta potential value of 4.70 mV. After DLSC, the MNPs become very negatively charged with an average zeta potential of –42.6 mV, which is consistent with the reported value of silica particles at this pH.[29] This finding confirms a full surface coverage of silica films on the MNPs by DLSC. The silanation of silica-coated

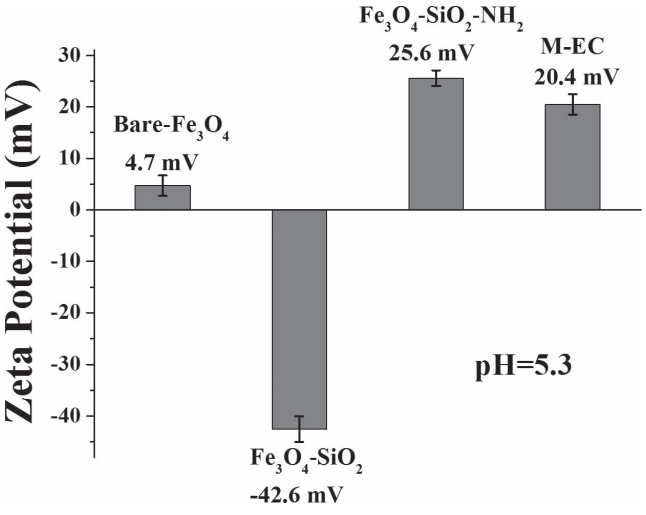


**Figure 3.** Zeta potentials of different particles in 1 mM KCl solutions.

$Fe_3O_4$ nanoparticles by 3-APTES makes the silica-coated, negatively charged nanoparticles to be strongly positively charged with an average zeta potential of 25.6 mV. Such reverse in zeta potential by 3-APTES silanation confirms not only the coupling of 3-APTES on silica-coated MNPs, but also the orientation of $–NH_2$ terminal groups towards the external surfaces, i.e., $Fe_3O_4$-$SiO_2$-$NH_2$, allowing the exposed amine groups to be reactive on the surface. The results are in line with those reported previously.[16,28] The reaction of bromoesterified-EC with amine-functionalized MNPs reduced the zeta potential value from 25.6 mV to 20.4 mV for the final product M-EC. Considering the experimental errors of zeta potential measurements, as shown in Figure 3, the difference of 5.2 mV in the zeta potential values of $Fe_3O_4$-$SiO_2$-$NH_2$ and M-EC is significant and the only difference between the two samples is the grafting of EC on $Fe_3O_4$-$SiO_2$-$NH_2$, which indirectly confirms the graft of EC on $Fe_3O_4$-$SiO_2$-$NH_2$. The shift of the zeta potential to a less positive value is attributed to the reduction in protonated (positive charge) $–NH_2$ groups on the surface of the $Fe_3O_4$-$SiO_2$-$NH_2$ nanoparticles as a result of reactions of protons on $–NH_2$ groups with $Br^–$ on EC, which reduces the surface concentration of the protonated $–NH_2$ groups, and hence the positive surface charge density. The results from zeta potential measurements provide convincing evidence that each step during the synthesis of M-EC changes the surface properties as anticipated.

### 2.1.3. Fourier-Transform Infrared Spectroscopy Studies

To further confirm the binding of bromoesterified-EC on 3-APTES silanized MNPs, the particles collected at various stages of synthesis were characterized using diffuse reflectance infrared Fourier-transform spectroscopy (DRIFTS). Spectrum (4b) of bare $Fe_3O_4$ nanoparticles, shown in **Figure 4**, has only two distinct bands at 3453 and 656 $cm^{-1}$. These two bands are attributed to vibrations of FeO–H and Fe–O bonds, respectively. After DLSC coating of $Fe_3O_4$ nanoparticles, strong bands in spectrum (4c) at 3745 $cm^{-1}$ are observed. These bands originate from Si–OH

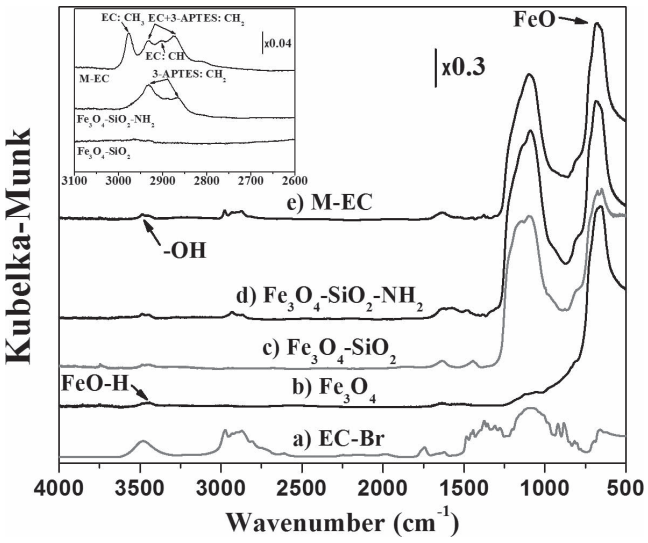


**Figure 4.** DRIFTS spectra of a) EC-Br, b) bare $Fe_3O_4$, c) $Fe_3O_4$-$SiO_2$, d) $Fe_3O_4$-$SiO_2$-$NH_2$, and e) M-EC. The inset shows a narrow scan the DRIFTS spectra of (c–e), confirming the silica coating (c), 3-APTES silanation (d), and EC grafting (e).

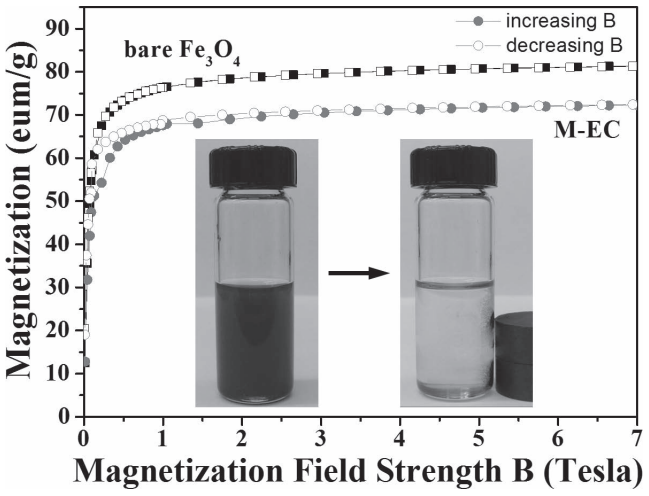


**Figure 5.** Room-temperature magnetization of MNPs without (bare $Fe_3O_4$) and with EC (M-EC), showing a noticeable reduction in the saturation magnetization by silica coating and EC-grafting of MNPs in addition to the superparamagnetic characteristics of M-EC. The photographs shows the magnetic response of M-EC in heavy naphtha to a hand magnet.

vibrations, indicating the presence of the silica coating. Spectrum (4e) of M-EC, shows three distinct bands at 3487, 2977, and 1377 $cm^{-1}$. These bands are also observed in spectrum (4a) of bromoesterified EC, and they are attributed to stretching of the –OH group and stretching and bending of the $–CH_3$ group, respectively. The close match of these two spectra confirms the successful grafting of bromoesterified EC on 3-APTES silanized MNPs. As shown in the inset of Figure 4, there is a clear spectral difference over the wavelength range from 3000 to 2800 $cm^{-1}$ among the spectra of $Fe_3O_4$-$SiO_2$, $Fe_3O_4$-$SiO_2$-$NH_2$, and M-EC nanoparticles. There are no characteristic bands in the spectrum of silica-coated MNPs, $Fe_3O_4$-$SiO_2$. After silanation of the silica-coated MNPs by 3-APTES, two distinct bands at 2877 and 2970 $cm^{-1}$ from asymmetric and symmetric stretching of $–CH_2$ groups are observed, signifying the anchoring of 3-APTES on silica-coated $Fe_3O_4$ nanoparticles. Unfortunately, the bands corresponding to $–NH_2$ vibrations are not observed due to the extremely weak nature of the bands. For the spectrum of M-EC, in addition to the spectral features described above, vibrational bands at 2977 and 2902 $cm^{-1}$ corresponding to $–CH_3$ and –CH on the glucose rings are observed. These spectral features confirm the success of EC grafting on 3-APTES silanized MNPs.

### 2.1.4. Magnetization Measurements

For the intended applications of magnetic dewatering and preparing magnetically responsive emulsions, it is important that the synthesized MNPs remain superparamagnetic so that they can be effectively separated from a complex multiphase system or readily manipulated by an external magnetic field. The magnetic property is clearly one of the key features of interfacially active MNPs. The magnetic properties of bare $Fe_3O_4$ and M-EC were determined and the results are shown in **Figure 5**. Compared with bare $Fe_3O_4$ nanoparticles, which have a saturation magnetization of 80 emu $g^{-1}$, the silica coating and EC grafted M-EC of similar average particle size (≈40 nm) showed a saturation magnetization of 71 emu $g^{-1}$. The reduction in the saturation magnetization of M-EC is most likely caused by the coating of diamagnetic thin silica films, further confirming successful coating of silica on $Fe_3O_4$ nanoparticles. Despite an 11% reduction in the saturation magnetization, the M-EC still remains magnetically responsive that it can be effectively manipulated by or attracted to a magnet, as shown in the photograph in Figure 5. More importantly, the MNPs remain superparamagnetic after grafting of EC. As a result, the M-EC nanoparticles exposed to an external magnetic field can rapidly be redispersed after the removal of external magnetic field for regeneration and recycle.

### 2.1.5. Thermogravimetric Analysis

The amount of the organic compound on the surface of the MNPs was determined by thermogravimetric analysis (TGA). A weight loss over a given temperature range can be attributed to the phase transformation of solids or decomposition of the organic substances, depending on the exact temperature at which the weight loss occurs. The TGA results in **Figure 6** show a negligible weight loss over the temperature range up to 800 °C for bare $Fe_3O_4$, $Fe_3O_4$-$SiO_2$, and $Fe_3O_4$-$SiO_2$-$NH_2$, indicating the absence of phase transformation and decomposition, and hence few organic compounds on the surface of these MNPs. In contrast, a significant weight loss of around 5 wt% is observed when M-EC nanoparticles are heated to ≈300 °C. This weight loss could be attributed to the decomposition of EC grafted on MNPs. To confirm this hypothesis, the decomposition of bulk EC was investigated by TGA. The TGA thermogram of EC in Figure 6 shows an incipient temperature of 300 °C where the significant weight loss starts. At 400 °C, a weight loss of 95% is observed, indicating an almost complete decomposition. The amount of EC grafted on the MNPs is therefore estimated to be about 50 mg $g^{-1}$.

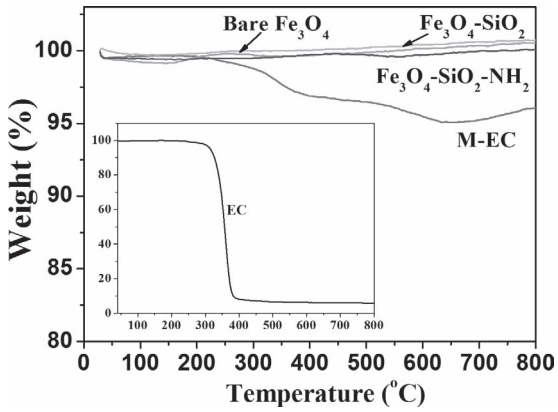


**Figure 6.** TGA curves for M-EC, bare-$Fe_3O_4$, $Fe_3O_4$-$SiO_2$-$NH_2$, and $Fe_3O_4$-$SiO_2$. The inset shows the TGA curve for EC.

### *2.1.6. Interfacial Activity of M-EC Nanoparticles*

The M-EC nanoparticles synthesized following the procedures described above are found to be better dispersed in organic solvents (e.g., chloroform, heavy naphtha, and toluene) than that in water due to the presence of EC (an oil-soluble polymer) on the surface of the MNPs. In order to demonstrate the interfacial activity of the synthesized M-EC nanoparticles, M-EC in heavy naphtha suspension was prepared. The suspension was found stable over an extended period of time (≈1 h). The resulting suspension was placed on the top of water as shown in **Figure 7**a. M-EC nanoparticles in the suspension migrated gradually to and stayed at the heavy naphtha/water interface over 1 h. Interestingly, these M-EC nanoparticles stayed at the heavy naphtha/water interface without further settling/diffusing into the water phase for a three-month period, clearly demonstrating the interfacial activity of M-EC. In contrast, when the suspension of the original $Fe_3O_4$ nanoparticles in heavy naphtha was placed on water, the MNPs without EC transported under gravity across the heavy naphtha/water interface into the aqueous phase and eventually settled to the bottom of the test vial, as shown in Figure 7b. We also found that $Fe_3O_4$-$SiO_2$ and $Fe_3O_4$-$SiO_2$-$NH_2$ exhibited a similar behavior to the original $Fe_3O_4$ nanoparticles. It is evident that the interfacial activity of M-EC is due to the interfacial performance of EC grafted on 3-APTES silanized MNPs.

To further understand interfacial activity of M-EC MNPs, the Langmuir–Blodgett technique was applied to study the M-EC at

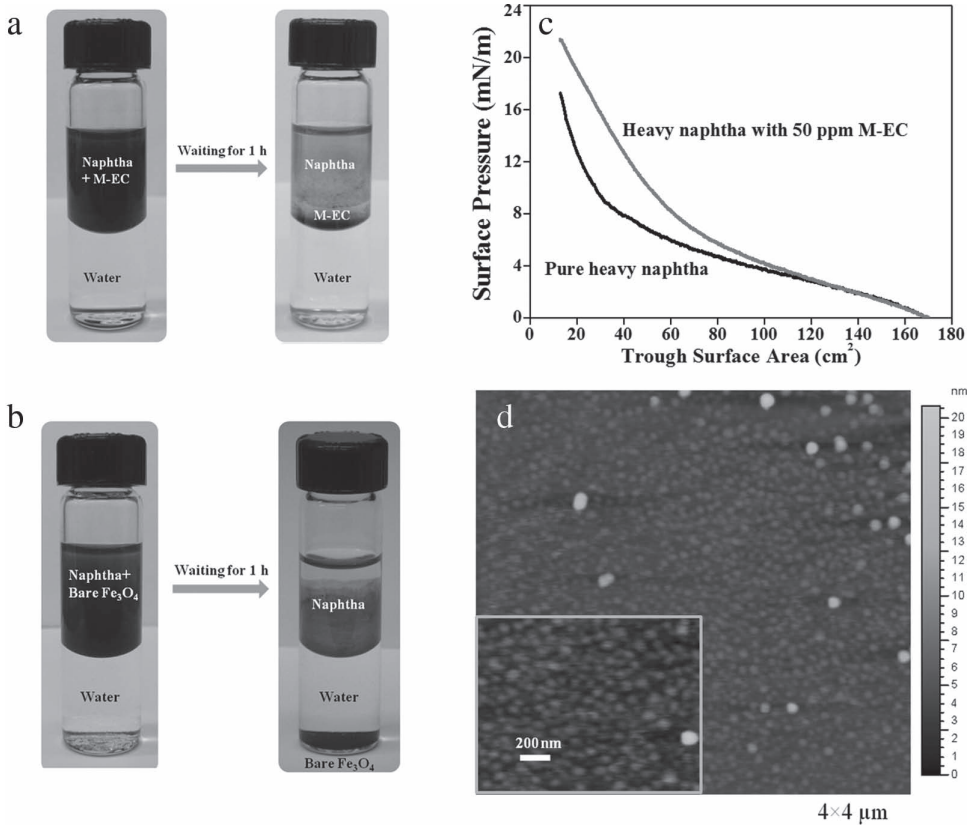


**Figure 7.** a) Photograph of M-EC in heavy naphtha as a dark dispersion resting on the top of water, showing the transfer and accumulation of interfacially active M-EC nanoparticles at the heavy naphtha/water interface after 1 h sedimentation. b) Photograph of bare $Fe_3O_4$ in the heavy naphtha as a dark dispersion resting on the top of water, indicating the transfer of hydrophilic MNPs across the heavy naphtha/water interface into the aqueous phase and settling to the bottom of the testing vial after 1 h. c) Interfacial pressure–area isotherm of M-EC nanoparticles at the heavy naphtha/water interface, showing surface activity of M-EC at heavy naphtha/water interface without apparent phase transition. d) AFM image of M-EC transferred at 15 mN $m^{-1}$ interfacial pressure from heavy naphtha/water interface by Langmuir–Blodgett technique. The inset shows close-packing morphology of M-EC at the heavy naphtha/water interface. The scale bar in the inset is 200 nm.

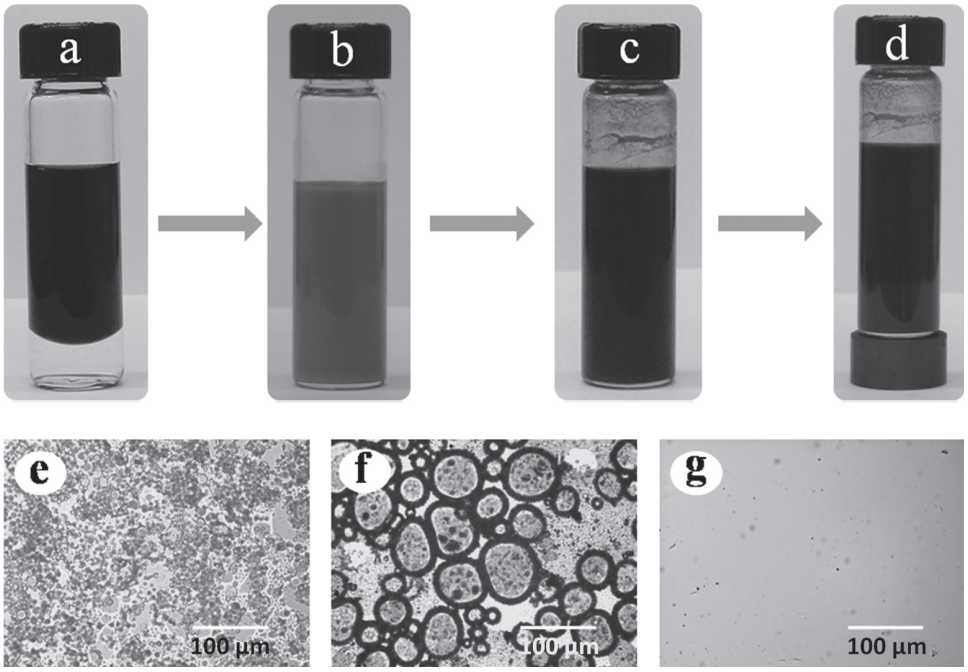


**Figure 8.** Photographs of a) asphaltene in toluene solution as a dark solution resting on the top of water; b) stable water in asphaltene-in-toluene emulsion emulsified from (a); c) addition of M-EC suspension into emulsion (b); and d) phase separation of emulsified water from asphaltene-in-toluene solution with a hand magnet. Microscopy images of e) stable emulsions from bottle (b), showing well-dispersed water droplets in asphaltene-in-toluene solution; f) water droplets with attached MNPs at the bottom of the bottle (d), showing enhanced coalescence of emulsified water droplets by magnetic forces of M-EC under external magnetic field; and g) the oil phase at the top from bottle (d), showing the absence (removal) of the emulsified water droplets observed in (e) by the hand magnet.

heavy naphtha/water interfaces. The pressure–area isotherm in Figure 7c shows a higher interfacial pressure for a given interfacial area with M-EC nanoparticles than that without M-EC nanoparticles, suggesting the stable occupancy of M-EC nanoparticles at the heavy naphtha/water interface even under the constraint interfacial conditions and hence surface activity of M-EC nanoparticles. It is interesting to note a more compressive nature of heavy naphtha/water interface with M-EC than that without M-EC as illustrated by a small increase of surface pressure with decreasing interfacial area. No apparent phase transition or collapse point was observed upon compression up to 20 mN $m^{-1}$.[30]

To confirm M-EC nanoparticles remained at the heavy naphtha/water interface, the materials at the heavy naphtha/water interface were transferred to a silica wafer at the interfacial pressure of 15 mN $m^{-1}$. The typical atomic force microscopy (AFM) image in Figure 7d shows a compact monolayer of the M-EC nanoparticles at the heavy naphtha/M-EC/water interface. The size of most M-EC nanoparticles remained ≈40–50 nm, which is in good agreement with the SEM imaging results of M-EC nanoparticles dispersed in organic solvents. The outstanding interfacial activity of M-EC nanoparticles makes them arranged in a high order at the heavy naphtha/water interface.

### 2.2. Application of Interfacially Active and Magnetically Responsive M-EC to Enhanced Demulsification

As an example, the interfacially active M-EC nanoparticles were applied to enhancing the coalescence of stable water droplets emulsified in asphaltene-in-toluene solution and the separation of water droplets from the organic phase by magnetic separation. As shown in **Figure 8**a,b, a toluene/water (4:1, w/w) emulsion is prepared with asphaltene (0.2 wt% of asphaltene in toluene) as the emulsion stabilizer.[31] This emulsion is stable for at least 30 min without any visible phase separation. Because of their interfacial activity, the magnetic M-EC nanoparticles added are able to attach to the water droplets in emulsions. As a result, M-EC-labeled water droplets move towards the bottom of the test vial under the attraction of an external magnetic field, leading to a rapid phase separation of emulsified water from the organic phase in less than 10 s, as shown in Figure 8c,d. As shown in Figure 8d, the concentrated water droplets at the bottom of the test vial remain dark, suggesting the presence of dark stabilizing asphaltene molecules at the oil/water interface. Nevertheless, microscopy images clearly show the rapid separation of aqueous phase from the organic phase by the hand magnet. Such rapid separation was not observed without applying an external magnetic field, demonstrating the important role of tagging the water droplets with magnetically responsive M-EC nanoparticles in the demulsification.

To understand the mechanism of water removal from emulsions by M-EC nanoparticles, emulsion systems were investigated using an optical microscope. As shown in Figure 8e, the water droplets in the system shown in Figure 8b are indeed in the form of emulsions with the droplets smaller than 10 μm in diameter. In contrast, the size of the water droplets at the bottom of the system after treatment with M-EC increased

sharply, as shown in Figure 8f. It is evident that EC on the surface made the MNPs interfacially active. These particles accumulated at the oil/water interface. Under an external magnetic field from a hand magnet, magnetic forces applied on the M-EC nanoparticles enhanced the coalescence of water droplets and their rapid migration to the magnet on the bottom of the vial. As a result, a clean organic phase without visible water droplets, as shown in Figure 8g, was obtained. The experimental results clearly demonstrate an excellent interfacial activity of M-EC nanoparticles prepared in this study and their responsive nature to an external magnetic field. Unlike traditional coalescence processes using chemical demulsifiers such as polymers,[32] imparting the magnetic properties of M-EC to water droplets could enhance coalescence with an applied external magnetic field. More importantly, the coalescence is not necessary with M-EC, as magnetically tagged water droplets can be effectively isolated from the complex multiphase systems by an external magnetic field, leading to a much more rapid separation of emulsified water from oil by a magnetic separator. Our study also showed a much reduced volume of the sludge of separated water due to enhanced coalescence by the external magnetic field, leading to less oil loss and consequently waste disposal. Furthermore, the spent M-EC can be easily recovered by magnetic methods and therefore reused with or without regeneration. It is anticipated that this type of magnetically responsive, interfacially active MNPs will have a long-lasting impact on life science, natural science, environmental science, and engineering practices.

## 3. Conclusions

In this study, an interfacially active, magnetically responsive nanoparticle, M-EC, was designed and synthesized by chemical coupling of a specially designed polymer on surface-modified $Fe_3O_4$ nanoparticles. The graft of an interfacially active EC on 3-APTES silanized MNPs was confirmed by zeta potential measurements, DRIFTS analysis, and TGA. SEM imaging showed a negligible increase in particle size and good dispersion after surface treatment. The magnetic response of M-EC was determined by room-temperature magnetization measurements. The pressure–area interfacial isotherm combined with AFM imaging of the Langmuir–Blodgett interfacial film showed a high interfacial activity and the formation of a compact film of M-EC at heavy naphtha/water interface. The interfacial activity of M-EC nanoparticles allows them to effectively attach to water droplets in emulsions, while strong magnetic properties of the $Fe_3O_4$ core provide quick and effective separation of the emulsified water droplets from the multiphase systems by magnetic separation. More importantly, the magnetic response of M-EC at the oil/water interfaces enhances coalescence of emulsified water droplets in toluene stabilized by asphaltenes. To the best of our knowledge, this is the first report on the synthesis of interfacially active and magnetically responsive nanoparticles containing a magnetic core and an interfacially active polymer layer. These magnetically responsive, interfacially active MNPs are anticipated to have long-lasting impact on life science, natural science, environmental science, and engineering practices.

## 4. Experimental Section

*Materials*: Magnetite (98% $Fe_3O_4$, <50 nm, with average primary particle size of ≈40 nm), 2-bromoisobutyryl bromide, and 3-APTES (99%) were purchased from Sigma-Aldrich. EC (ethoxyl content 48%, 4 cps), pyridine (99.5%, extra dry), tetrahydrofuran (THF, 99.5%, extra dry), and toluene (99.8%, extra dry) were purchased from Acros Organics. $Na_2SiO_3{\cdot}9H_2O$ was purchased from Fisher Scientific. All solvents and chemicals were used as received without further purification. Millipore deionized water (Millipore, Canada) was used whenever needed.

*Preparation of EC-Br*: The bromoesterified ethyl cellulose (EC-Br) was prepared according to the procedures described in a previous report.[27] EC (8.0784 g, 40 mmol) was dissolved in THF (200 mL), followed by the addition of pyridine (0.81 mL, as HBr absorbent). The mixture was then stirred at 0 °C. The THF solution (10 mL) containing 2-bromoisobutyryl bromide (1.24 mL) was added dropwise to the above solution under stirring. After the completed addition of 2-bromoisobutyryl bromide to the THF solution, the mixture was heated to 40 °C with stirring for 3 h. The reaction mixture was then cooled to room temperature and stirred for 24 h. After the completion of reaction, the mixture was filtered. The EC-Br was precipitated out of the filtrate by adding to deionized water. The solid collected was dissolved in THF and re-precipitated in deionized water to give a desired product in ≈90% yield as a white or yellowish powder.

*Preparation of Amino-Functionalized $Fe_3O_4$ Nanoparticles*: Silica coating of $Fe_3O_4$ was accomplished using the DLSC method. In this case, magnetite (3 g) was dispersed in deionized water (180 mL) by vigorous mechanical agitation in an ultrasonic bath for 30 min. 1 mol $L^{-1}$ sodium silicate solution (12.5 mL) was slowly added into the above suspension under mechanical stirring at 40 °C. To better control silica coating, the suspension pH, monitored with a pH meter (Fisher Scientific), was kept at 9.5 during this stage by the addition of 0.3 mol $L^{-1}$ $H_2SO_4$ aqueous solution. The suspension temperature was kept at 40 °C for 3 h and then raised to 95 °C for 1 h to dehydrate the suspension. The solid particles were then thoroughly washed three times with an ample amount of deionized water and collected each time using a hand magnet. To effectively hydrolyze the $Fe_3O_4$-$SiO_2$ surfaces, the $Fe_3O_4$-$SiO_2$ particles were steamed for 1 h with boiling deionized water. The hydrolyzed particles were recovered and baked for 1 h at 100 °C in a well-ventilated oven to remove free water. The sample was then mixed by vigorous stirring with toluene, followed by slow addition of 3-APTES (10 mL) under continuous mechanical stirring. Reaction under reflux was allowed to continue for 4 h. The resulting suspension of $Fe_3O_4$-$SiO_2$-$NH_2$ nanoparticles was cooled to room temperature and the particles were collected with a hand magnet. After successive washes with toluene and ethanol, the particles were dried in a vacuum oven at room temperature.

*Preparation of M-EC Nanoparticles*: $Fe_3O_4$-$SiO_2$-$NH_2$ (3 g) nanoparticles were dispersed in THF (150 mL) by mechanical agitation, and then pyridine (1 mL, as HBr absorbent) was added to the suspension. EC-Br (0.5 g) powder was added in the above suspension, the mixture was stirred at room temperature for 48 h. The resulting EC-grafted MNPs were washed with THF and dried in vacuum to obtain the desired M-EC nanoparticles.

*Characterization of M-EC Nanoparticles*: SEM imaging of the MNPs was performed on a JAMP-9500F field-emission Auger Microprobe (JEOL). The accelerating voltage was 25 kV. The SEM sample was prepared by placing a few drops of dilute MNPs in $CHCl_3$ suspension onto a carbon-coated copper grid.

The zeta-potentials of the MNPs at various stages of the synthesis were measured in 1 mM KCl background electrolyte solution using a Zeta Sizer (Nano ZS 3600, Nano Series, Malvern). The nanoparticles were dispersed in KCl solutions. The suspension was used for zeta potential measurements.

DRIFTS with an FTS 6000 spectrometer (Bio-Rad Laboratories) was used to acquire Fourier transform infrared (FTIR) spectra of powder particles in the spectral range of 4000 to 400 $cm^{-1}$. A sample of finely crushed KBr was used as the background. All spectra were obtained

using 128 scans at a nominal resolution of 4.0 $cm^{-1}$ and were presented without background correction.

The TGA was performed on a STA 409 PC thermogravimetric analyzer (NETZSCH instruments). Samples between 10 and 15 mg were heated from 40 to 800 °C at a heating rate of 10 °C $min^{-1}$ in a $N_2$ atmosphere.

The magnetic properties of the magnetite particles before and after treatment were measured with a Quantum Design PPMS 9T magnetometer/susceptometer. The measurements were conducted at room temperature with a magnetization field strength cycling from 0 to 7 Tesla and back to 0 Tesla.

*Interfacial Activity Measurements*: Langmuir–Blodgett films were prepared using a Langmuir interfacial trough (KSV instruments, Finland). The trough and barriers were rinsed with high-performance liquid chromatography (HPLC)-grade toluene prior to each experiment. The interfacial pressure was measured with a Wilhelmy plate (Whatman 1 CHR filter paper) attached to a microbalance. Heavy naphtha (Champion Technologies Inc.) was used as the top phase in this set of experiments. The interfacial films at heavy naphtha/water interface were transferred onto hydrophilic silicon wafers using the Langmuir–Blodgett technique. In each test, the lower compartment of the Langmuir interfacial trough was first filled with 120 mL of Milli-Q water as the subphase. The water subphase was considered clean if the pressure sensor reading was below 0.2 mN $m^{-1}$ upon the compression of the barriers to the closest position. After obtaining the appropriate level of cleanliness, a clean and dry silicon wafer was immersed in the water subphase. As the top phase, a mixture of 5 mg of M-EC nanoparticles dispersed in 100 mL of heavy naphtha by ultrasonication for 1 min was added slowly onto the water surface using a glass funnel. The compression of the interfacial film started after 10 min equilibration.

Silicon wafers used as substrate in this study were purchased from NanoFab (University of Alberta). They were polished on one side and 0.5 µm in thickness and 10 cm in diameter. Prior to their use, they were cut to $1 \times 3$ $cm^2$ pieces and cleaned by soaking in a 70/30 by volume solution of 96% sulfuric acid and 30% hydrogen peroxide at 90 °C for 30 min, followed by thorough rinsing with Milli-Q water. The cleaned silicon wafer was stored in Milli-Q water prior to its use. The interfacial film at heavy naphtha/water interface was transferred to a silicon wafer under a constant interfacial pressure of 15 mN $m^{-1}$ and pulling rate of 5 mm $s^{-1}$, resulting in a typical transfer ratio of 2.6. The prepared films were imaged by AFM.

AFM images of Langmuir–Blodgett films were obtained using a multimode atomic force microscope with a nanoscope IIIa controller (Veeco, Santa Barbara, CA) operating under tapping mode in air. AFM imaging was carried out at room temperature (20 °C ± 0.5 °C) using a multimode scanning probe microscope head and a J-scanner. A silicon nitride tip (RTESP, Veeco) with a resonance frequency of 260–320 kHz was used for imaging at the scan rate of 1 Hz. Images were obtained at several locations for each sample.

*Stability Measurements of Emulsions*: The water-in-toluene emulsion for this experiment was prepared using a homogenizer (PowerGen homogenizer, 125 W) operating at 30 000 rpm for 3 min. The asphaltene (0.2 wt% in toluene) was used as the stabilizer of the emulsions. Asphaltenes were precipitated from bitumen by adding 40 times n-heptane to bitumen by volume. Details about the asphaltene precipitation can be found elsewhere.[33] The ratio of water to asphaltene in the toluene solution was kept at 1:4 w/w. The demulsification was accomplished by homogenizing 0.05 g of M-EC in 5 g of emulsion in a 10 mL vial by a vortex mixer for 3 min. The resultant mixture was placed on a hand magnet. The fast motion of the M-EC tagged water droplets towards the magnet was visible. The separation was completed in 10 s. Microscopy images of the emulsions were obtained using a Carl Zeiss Axioskop 40 Pol microscope equipped with a video camera and interfaced with a personal computer. The emulsion sample, without further dilution, was placed on a glass slide and covered by a thin glass cover slide (25 mm × 25 mm × 0.2 mm). The image was acquired under a halogen light. The samples were taken from both the top and bottom of emulsions.

## Acknowledgements

The financial support for this work from Natural Sciences and Engineering Research Council of Canada under Industrial Research Chair program in Oil Sands Engineering is gratefully acknowledged. The authors thank Champion Technologies Inc. for providing the heavy naphtha. They also thank Prof. Arthur Mar's group in the Department of Chemistry at the University of Alberta for collecting the magnetization data. The support from Canadian Foundation for Innovation (CFI) for purchasing field emission scanning Auger spectrometer, atomic force microscope, and other facilities used in this study is also greatly appreciated.

Received: September 12, 2011
Revised: November 30, 2011
Published online: February 13, 2012

[1] a) A. H. Lu, E. L. Salabas, F. Schüth, *Angew. Chem. Int. Ed.* **2007**, *46*, 1222; b) S. L. Gai, P. P. Yang, C. X. Li, W. X. Wang, Y. L. Dai, N. Niu, J. Lin, *Adv. Funct. Mater.* **2010**, *20*, 1; c) A. K. Gupta, M. Gupta, *Biomaterials* **2005**, *26*, 3995; d) H. W. Gu, K. M. Xu, C. J. Xu, B. Xu, *Chem. Commun.* **2006**, *9*, 941; e) R. Hao, R. J. Xing, Z. C. Xu, Y. L. Hou, S. Gao, S. H. Sun, *Adv. Mater.* **2010**, *22*, 2729.

[2] a) A. H. Fu, W. Hu, L. Xu, R. J. Wilson, H. Yu, S. J. Osterfeld, S. S. Gambhir, S. X. Wang, *Angew. Chem. Int. Ed.* **2009**, *48*, 1620; b) C. T. Chen, Y. C. Chen, *Chem. Commun.* **2010**, *46*, 5674.

[3] a) M. Sureshkumar, D. Y. Siswanto, C. K. Lee, *J. Mater. Chem.* **2010**, *20*, 6948; b) J. Kim, H. S. Kim, N. Lee, T. Kim, H. Kim, T. Yu, I. C. Song, W. K. Moon, T. Hyeon, *Angew. Chem. Int. Ed.* **2008**, *47*, 8438; c) S. S. Banerjee, D. H. Chen, *Chem. Mater.* **2007**, *19*, 6345.

[4] a) F. M. Kievit, O. Veiseh, N. Bhattarai, C. Fang, J. W. Gunn, D. Lee, R. G. Ellenbogen, J. M. Olson, M. Q. Zhang, *Adv. Funct. Mater.* **2009**, *19*, 2244; b) K. Kang, J. Choi, J. H. Nam, S. C. Lee, K. J. Kim, S. W. Lee, J. H. Chang, *J. Phys. Chem. B* **2009**, *113*, 536; c) L. R. Yang, C. Guo, S. Chen, F. Wang, J. Wang, Z. T. An, C. Z. Liu, H. Z. Liu, *Ind. Eng. Chem. Res.* **2009**, *48*, 944.

[5] a) L. Wang, K. G. Neoh, E. T. Kang, B. Shuter, S. C. Wang, *Adv. Funct. Mater.* **2009**, *19*, 2615; b) D. L. Shi, H. S. Cho, Y. Chen, H. Xu, H. C. Gu, J. Lian, W. Wang, G. K. Liu, C. Huth, L. M. Wang, R. C. Ewing, S. Budko, G. M. Pauletti, Z. Y. Dong, *Adv. Mater.* **2009**, *21*, 2170; c) Z. L. Cheng, D. L. J. Thorek, A. Tsourkas, *Angew. Chem. Int. Ed.* **2010**, *49*, 346.

[6] a) S. S. Liu, H. M. Chen, X. H. Lu, C. H. Deng, X. M. Zhang, P. Y. Yang, *Angew. Chem. Int. Ed.* **2010**, *49*, 7557; b) H. M. Chen, C. H. Deng, Y. Li, Y. Dai, P. Y. Yang, X. M. Zhang, *Adv. Mater.* **2009**, *21*, 2200; c) Y. C. Li, Y. S. Lin, P. J. Tsai, C. T. Chen, W. Y. Chen, Y. C. Chen, *Anal. Chem.* **2007**, *79*, 7519.

[7] a) K. El-Boubbou, C. Gruden, X. F. Huang, *J. Am. Chem. Soc.* **2007**, *129*, 13392; b) C. G. Wang, J. Irudayaraj, *Small* **2010**, *6*, 283.

[8] a) D. K. Yi, S. T. Selvan, S. S. Lee, G. C. Papaefthymiou, D. Kundaliya, J. Y. Ying, *J. Am. Chem. Soc.* **2005**, *127*, 4990; b) J. P. Ge, H. Lee, L. He, J. Kim, Z. D. Lu, H. Kim, J. Goebl, S. Kwon, Y. D. Yin, *J. Am. Chem. Soc.* **2009**, *131*, 15687.

[9] a) M. Sari, S. Akgöl, M. Karatas, A. Denizli, *Ind. Eng. Chem. Res.* **2006**, *45*, 3036; b) D. K. Yi, S. S. Lee, J. Y. Ying, *Chem. Mater.* **2006**, *18*, 2459; c) W. Wang, Y. Xu, D. I. C. Wang, Z. Li, *J. Am. Chem. Soc.* **2009**, *131*, 12892; d) J. P. Ge, Q. Zhang, T. R. Zhang, Y. D. Yin, *Angew. Chem. Int. Ed.* **2008**, *47*, 8924.

[10] a) G. D. Moeser, K. A. Roach, W. H. Green, P. E. Laibinis, T. A. Hatton, *Ind. Eng. Chem. Res.* **2002**, *41*, 4739; b) R. D. Ambashta, P. K. Wattal, *Sep. Sci. Technol.* **2006**, *41*, 925.

[11] a) P. G. Wu, J. H. Zhu, Z. H. Xu, *Adv. Funct. Mater.* **2009**, *14*, 345; b) Y. G. Zhao, H. Y. Shen, S. D. Pan, M. Q. Hu, Q. H. Xia, *J. Mater. Sci.* **2010**, *45*, 5291; c) J. Dong, Z. H. Xu, S. M. Kuznichi, *Adv.*

*Funct. Mater.* **2009**, *19*, 1268; d) Y. Shiraishi, G. Nishimura, T. Hirai, I. Komasawa, *Ind. Eng. Chem. Res.* **2002**, *41*, 5065.
[12] a) J. Philip, P. D. Shima, B. Raj, *Appl. Phys. Let.* **2008**, *92*, 043108; b) J. Philip, C. B. Rao, T. Jayakumar, *Meas. Sci. Technol.* **1999**, *10*, N71.
[13] a) G. L. Li, D. L. M. Zeng, L. Wang, B. Y. Zong, K. G. Neoh, E. T. Kang, *Macromolecules* **2009**, *42*, 8561; b) M. Lattuada, T. A. Hatton, *Langmuir* **2007**, *23*, 2158; c) V. Antochshuk, M. Jaroniec, *Chem. Mater.* **2000**, *12*, 2496.
[14] Q. X. Liu, Z. H. Xu, *Langmuir* **1995**, *11*, 4617.
[15] Q. X. Liu, Z. H. Xu, J. A. Finch, R. Egerton, *Chem. Mater.* **1998**, *10*, 3936.
[16] M. Takafuji, S. Ide, H. Ihara, Z. H. Xu, *Chem. Mater.* **2004**, *16*, 1977.
[17] a) P. G. Wu, J. H. Zhu, Z. H. Xu, *Adv. Funct. Mater.* **2004**, *14*, 345; b) J. Dong, Z. H. Xu, F. Wang, *Appl. Surf. Sci.* **2008**, *254*, 3522.
[18] a) H. W. Duan, D. Y. Wang, D. G. Kurth, H. Möhwald, *Angew. Chem. Int. Ed.* **2004**, *43*, 5639; b) D. Y. Wang, H. W. Duan, H. Möhwald, *Soft Matter* **2005**, *1*, 412; c) B. Y. Du, X. J. Chen, B. Zhao, A. X. Mei, Q. Wang, J. T. Xu, Z. Q. Fan, *Nanoscale* **2010**, *2*, 1684.
[19] a) E. W. Edwards, M. Chanana, D. Y. Wang, H. Möhwald, *Angew. Chem. Int. Ed.* **2008**, *47*, 320; b) H. M. Yang, H. J. Lee, K. S. Jang, C. W. Park, H. W. Yang, W. D. Heo, J. D. Kim, *J. Mater. Chem.* **2009**, *19*, 4566; c) M. M. Lin, S. H. Li, H. H. Kim, H. Kim, H. B. Lee, M. Muhammed, D. K. Kim, *J. Mater. Chem.* **2010**, *20*, 444; d) A. Prakash, H. G. Zhu, C. J. Jones, D. N. Benoit, A. Z. Ellsworth, E. L. Bryant, V. L. Colvin, *ACS Nano* **2009**, *3*, 2139.
[20] a) D. Y. Chen, N. J. Li, H. W. Gu, X. W. Xia, Q. F. Xu, J. F. Ge, J. M. Lu, Y. G. Li, *Chem. Commun.* **2010**, *46*, 6708; b) X. Y. Shi, S. H. Wang, S. D. Swanson, S. Ge, Z. Y. Cao, M. E. V. Antwerp, K. J. Landmark, J. R. Baker Jr., *Adv. Mater.* **2008**, *20*, 1671; c) B. S. Kim, J. M. Qiu, J. P. Wang, T. A. Taton, *Nano Lett.* **2005**, *5*, 1987.
[21] a) B. Brugger, W. Richtering, *Adv. Mater.* **2007**, *19*, 2973; b) L. T. Romankiw, *US Patent 39810844*, **1976**.
[22] a) L. Zhang, P. Liu, T. M. Wang, *Chem. Eng. J.* **2011**, *171*, 711; b) I. Kalashnikova, H. Bizot, B. Cathala, *Langmuir* **2011**. *27*, 7471; c) J. Zhou, X. Y. Qiao, B. P. Binks, K. Sun, M. W. Bai, Y. L. Li, Y. Liu, *Langmuir* **2011**. *27*, 3308.
[23] a) K. Moran, J. Czarnecki, *Colloids Surf. A* **2007**, *292*, 87; b) L. Y. Zhang, Z. H. Xu, J. H. Masliyah, *Langmuir* **2003**, *19*, 9730; c) A. Yeung, T. Dabros, J. H. Masliyah, *Langmuir* **1998**, *13*, 6597.
[24] a) D. Klemm, B. Heublein, H.-P. Fink, A. Bohn, *Angew. Chem. Int. Ed.* **2005**, *44*, 3358; b) M. M. Crowley, B. Schroeder, A. Fredersdorf, S. Obara, M. Talarico, S. Kucera, J. W. McGinity, *Int. J. Pharm.* **2004**, *269*, 509; c) X. G. Li, I. Kresse, Z. K. Xu, J. Springer, *Polymer* **2001**, *42*, 6801.
[25] X. H. Feng, Z. H. Xu, J. H. Masliyah, *Energy Fuels* **2009**, *23*, 451.
[26] a) X. H. Feng, P. Mussone, S. Gao, S. Q. Wang, S. Y. Wu, J. H. Masliyah, Z. H. Xu, *Langmuir* **2010**, *26*, 3050; b) S. Q. Wang, J. J. Liu, L. Y. Zhang, J. H. Masliyah, Z. H. Xu, *Langmuir* **2010**, *26*, 182.
[27] a) Y. Shiraishi, G. Nishimura, T. Hirai, I. Komasawa, *Ind. Eng. Chem. Des.* **2002**, *41*, 5065; b) X. H. Xu, Q. X. Liu, J. A. Finch, *Appl. Surf. Sci.* **1997**, *120*, 269.
[28] H. L. Kang, W. Y. Liu, B. Q. He, D. W. Shen, L. Ma, Y. Huang, *Polymer* **2006**, *47*, 7927.
[29] P. G. Wu, Z. H. Xu, *Ind. Eng. Chem. Res.* **2005**, *44*, 816.
[30] a) Y. J. Shen, Y. L. Lee, Y. M. Yang, *J. Phys. Chem. B* **2006**, *110*, 9556; b) H. J. Tsai, Y. L. Lee, *Soft Matter* **2009**, *5*, 2962.
[31] B. M. Aguilera, J. G. Delgado, A. C. Cárdenas, *J. Dispersion Sci. Technol.* **2010**, *31*, 359.
[32] J. Philip, L. Bonakdar, P. Poulin, J. Bibette, F. Leal-calderon, *Phys. Rev. Lett.* **2000**, *84*, 2018.
[33] L. Y. Zhang, S. Lawrence, Z. H. Xu, J. H. Masliyah, *J. Colloid Interface Sci.* **2003**, *264*, 128.